Heliyon

Received:
23 September 2018
Revised:
7 December 2018
Accepted:
30 January 2019

Cite as: Azad Hussain, Sobia Akbar, Lubna Sarwar, Sohail Nadeem, Zaffar Iqbal. Effect of time dependent viscosity and radiation efficacy on a non-Newtonian fluid flow. Heliyon 5 (2019) e01203. doi: 10.1016/j.heliyon.2019.e01203

Effect of time dependent viscosity and radiation efficacy on a non-Newtonian fluid flow

Azad Hussain [a,*], **Sobia Akbar** [a], **Lubna Sarwar** [a], **Sohail Nadeem** [b], **Zaffar Iqbal** [a]

[a] *Department of Mathematics, University of Gujrat, Gujrat 50700, Pakistan*

[b] *Department of Mathematics, Quaid-i-Azam University, Islamabad 44000, Pakistan*

[*] Corresponding author.

E-mail address: azad.hussain@uog.edu.pk (A. Hussain).

Abstract

In the present article we have studied the radiation effects on the flow of a viscoelastic fluid flow past a spongy plate by considering the viscosity as variable. In order to explore the variable viscosity effects, law of conservation of mass, momentum and energy are flourished. The shooting method is adapted to accomplish the numerical solution of governing equations. The effects of the involved emerging parameters such as Reynolds' model viscosity numbers, Vogel's model viscosity numbers and Prandtl numbers on velocity and temperature profiles are discussed with the help of graphs. The associated physical properties of the flow i.e. the skin friction coefficient and Nusselt numbers are presented graphically for different parameters. The tables for effects of distinct parameters on temperature profile at the wall for Reynolds' model and Vogel's model are given. Impact of various parameters involved on Nusselt number and skin friction are also presented in tables.

Keywords: Applied mathematics, Mechanics

1. Introduction

Fluid Mechanics is the branch of the physical sciences which deals with the behavior of the fluids, whether they are moving or stationary. Fluid Mechanics plays an

https://doi.org/10.1016/j.heliyon.2019.e01203

important role to model the red spot on Jupiter, or predict the behavior of subatomic particles in a betatron, or measure the vorticity in a tornado, or design a transonic wing for a supersonic transport. It provides the base for aerodynamics, propulsion and combustion; meteorology, oceanography, and astronomy; for biofluids, acoustics and particle physics. Materials exhibiting non-Newtonian flow characteristics involve, soap solutions, biological fluids, natural products, polymer melts and solutions, dairy wastes and agricultural wastes, magmas and lavas, personal care products including toiletries and cosmetics, multiphase mixtures, food products, building materials etc. In literature a number of researchers [1, 2, 3, 4, 5, 6, 7, 8, 9, 10, 11, 12, 13, 14, 15, 16, 17, 18, 19, 20] studied radiation effects on fluid flow through different geometries and boundary conditions. The downright and coherent results of non-Newtonian fluids with variable viscosity was anatomized by Yursoy and Pakdemirili [21] and Pakdemirili and Yilbas [22].

The model of Walters' B fluid describes the behaviors of different polymeric liquids upon chemical engineering and biotechnology. The boundary layer flow of viscoelastic fluid close to a stagnation point was studied by Walter and Beard [23]. Walters' B equation as a simpler constitutive equation generates nonlinear initial value problems which are not trivial. Chang et al. [24] examined the numerical solution of Walters' B fluid of viscoelastic flow for free convective heat transfer. Nandeppanavar et al. [25] investigated the Walters' B fluid appearace of nonuniform heat source. Such analysis is extended by Hakeem et al. [26] acompany of radiation. Nadeem et al. [27] also analyzed the flow of Walters' B fluid of oblique flow in the existence of nanoparticles and magnetohydrodynamics. The Walters' B flow bounded by an increasing stretching sheet was given by Talla [28]. Ramesh and Devakar [29] discussed the peristalsis of Walters' B fluid through a vertical channel.

Radiation effects on boundary layer flow has much importance in engineering, physics and industries such as furnace aspire, polymer proceeding, space gas cooled nuclear reactors, glass handiwork and way technology. The merge backwash of linear and nonlinear radiation precipitate on stagnancy point over a stretching surface was analyzed by Hussain et al. [30]. The sway of thermal radiation sequel on heat flow athwart a pad sheet was studied by Cortell [31]. He engages the nonlinear Rosseland approach to assimilate the thermal radiation move. Motivated from the consequence of the fluid flow, the effects of radiation on steady flow of Walter's B fluid model with variable viscosity past a porous plate is studied. Numerical solution of the problem is obtained. The tables of temperature on effects of distinct parameters at the wall are given. Impact of various parameters involved on skin friction and Nusselt number are also presented in tables and graphs. Graphs of different emerging parameters are also presented. The problem is divided into two different parts in which first part explicates that the plate has greater temperature than fluid's temperature. Second part describes that plate is insulated. The results are also discussed at the end section.

https://doi.org/10.1016/j.heliyon.2019.e01203

2. Model

The cauchy stress tensor of Walter's B fluid is given by

$$S = -pI + 2\eta_0 \mathbf{e} - 2k_0 \frac{\delta \mathbf{e}}{\delta t}. \tag{1}$$

Here, p represents pressure, I identity tensor, η_0 is viscosity and a_0 is short memory coefficient, which are defined as

$$\eta_0 = \int_0^\infty N(\tau) d\tau, \quad k_0 = \int_0^\infty \tau N(\tau) d\tau. \tag{2}$$

where $N(\tau)$ represents the distribution function along with relaxation time τ.

In the present problem, we discussed the radiation effects on a viscoelastic Walters' B fluid model past an infinite pervious plate (Fig. 1).

Velocity and temperature fields figured out as

$$\mathbf{v} = u(x)i + w(x)k, \tag{3}$$

$$\theta = \theta(x). \tag{4}$$

As θ represents temperature, u and w indicates velocity components. The governing equations which are the conservation of mass, momentum and energy are,

$$\frac{\partial \rho}{\partial t} + \mathrm{div}(\rho \mathbf{v}) = 0, \tag{5}$$

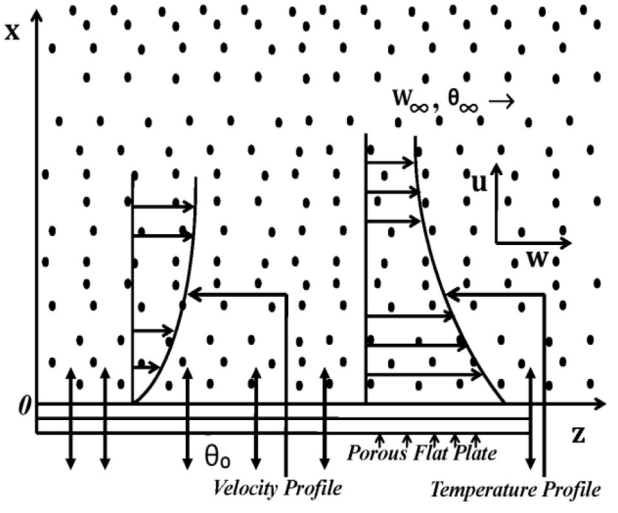

Fig. 1. Schematic figure of the problem.

https://doi.org/10.1016/j.heliyon.2019.e01203

$$\rho \frac{d\mathbf{v}}{dt} = \mathrm{div}(\mathrm{S}) + \rho\mathbf{f}, \tag{6}$$

$$\rho \frac{d\mathbf{e}}{dt} = S.L - \mathrm{div}(\mathbf{q}) + \rho\mathbf{r}, \tag{7}$$

where **b** is body force, ρ is fluid density, **e** shows internal energy, **q** heat flux vector, L represents velocity gradient and also **r** is signifies radiant heating. For incompressible fluid flow Eq. (5) becomes

$$\mathrm{div}\ \mathbf{v} = 0, \tag{8}$$

$$\mathrm{u} = -v_0 = Constant \tag{9}$$

where $v_0 > 0$ is suction and $v_0 < 0$ represents blowing at the plate. The governing momentum equation with viscosity as variable (in the absenteeism of body forces) for present problem may be written as

$$\frac{\partial P}{\partial z} = \rho v_0 \frac{dw}{dx} + \frac{d\mu_0}{dx}\frac{dw}{dx} + \mu_0 \frac{d^2w}{dx^2} + a_0 v_0 \frac{d^3w}{dx^3} \tag{10}$$

$$\frac{\partial P}{\partial x} = 2a_0 \frac{d}{dx}\left[\left(\frac{dw}{dx}\right)^2\right], \tag{11}$$

$$\frac{\partial P}{\partial y} = 0. \tag{12}$$

Now defining a modified pressure

$$\widehat{P} = P - (2\alpha_0)\left(\frac{dw}{dx}\right)^2. \tag{13}$$

The Eqs. (10), (11), and (12) can be written in the form

$$\frac{\partial \widehat{P}}{\partial z} = \rho v_0 \frac{dw}{dx} + \frac{d\mu_0}{dx}\frac{dw}{dx} + \mu_0 \frac{d^2w}{dx^2} + a_0 v_0 \frac{d^3w}{dx^3}, \tag{14}$$

$$\frac{\partial \widehat{P}}{\partial y} = 0, \tag{15}$$

$$\frac{\partial \widehat{P}}{\partial x} = 0 \tag{16}$$

Eq. (14) can be expressed as

https://doi.org/10.1016/j.heliyon.2019.e01203

$$\rho v_0 \frac{dw}{dx} + \frac{d\mu_0}{dx}\frac{dw}{dx} + \mu_0 \frac{d^2w}{dx^2} + a_0 v_0 \frac{d^3w}{dx^3} = P_1 \tag{17}$$

here

$$\frac{\partial \widehat{P}}{\partial z} = constant = P_1$$

Now the appropriate boundary conditions are

$$\mathrm{w}(0) = 0, \tag{18}$$

$$\mathrm{w}(x) \to \mathrm{W}_\infty \ \ as \ \ x \to \infty . \tag{19}$$

Since Eq. (17) is third-order equation, so more boundary conditions are required. As fluid is moving with uniform velocity. Far away from the plate so flow in free stream shear stress is zero. So,

$$S_{zx}|_{z\to\infty} = \left[\mu_0 \frac{d^2w}{dx^2} + a_0 v_0 \frac{d^3w}{dx^3}\right]_{x\to\infty} = 0. \tag{20}$$

We have necessary conditions i. e,

$$\frac{dw}{dx} = 0 \ \ when \ \ x \to \infty , \tag{21}$$

and also take another assumption that

$$P_1 = 0. \tag{22}$$

Now we concentrate on Eq. (7). Heat flux is

$$q = -k\left(\frac{\partial \theta}{\partial x}\right)_{x=0}. \tag{23}$$

And in Eq. (25). Radiation parameter is expressed as

$$q_r = -\frac{4\sigma^*}{3K^*}\frac{\partial \theta^4}{\partial x}. \tag{24}$$

The energy equation for the under consideration study takes the form

$$k\frac{d^2\theta}{dx^2} + \rho C_p v_0 \frac{d\theta}{dx} + \mu_0 \left(\frac{dw}{dx}\right) + v_0 a_0 \left(\frac{dw}{dx}\right)^2 \frac{d^2w}{dx^2} - \frac{1}{\rho C_p}\frac{\partial q_r}{\partial x} = 0. \tag{25}$$

Where C_p is specific heat.

https://doi.org/10.1016/j.heliyon.2019.e01203

The suitable boundary conditions for Eq. (25) are:

Case 1: Constant wall temperature

$$\theta(0) = \theta_0, \tag{26}$$

$$\theta(x) \to 0_\infty \ \ as \ \ x \to \infty . \tag{27}$$

Case b: Insulated wall

$$\left.\frac{d\theta}{dx}\right|_{x\to 0} = 0, \tag{28}$$

$$\theta(x) \to \theta_\infty \ \ as \ \ x \to \infty . \tag{29}$$

Solution for constant wall temperature

We define non-dimensional parameters

$$\overline{X} = \frac{X}{L}, \overline{w} = \frac{w}{W_\infty}, \overline{\theta} = \frac{\theta - \theta_\infty}{\theta_0 - \theta_\infty}, \tag{30}$$

where

$$L = \frac{k_0 v_0}{\mu_0^*}, \tag{31}$$

is the characteristic "length" and also

$$\overline{\mu_0} = \frac{\mu_0}{\mu_0^*} \tag{32}$$

Using above relations Eqs. (17) and (25) becomes

$$\frac{d^3\overline{w}}{d\overline{x}^3} + \mu_0 \frac{d^2\overline{w}}{d\overline{x}^2} + \gamma \frac{d\overline{w}}{d\overline{x}} + \frac{d\mu_0}{d\overline{x}} \frac{d\overline{w}}{d\overline{x}} = P_2, \tag{33}$$

$$\left(1 + \frac{4}{3}R\right) \frac{d^2\overline{\theta}}{d\overline{x}^2} + \gamma \mathrm{Pr} \frac{d\overline{\theta}}{d\overline{x}} + \lambda \mu_0 \left(\frac{d\overline{w}}{d\overline{x}}\right)^2 + \lambda \left(\frac{d\overline{w}}{d\overline{x}}\right) \frac{d^2\overline{w}}{d\overline{x}^2} = 0. \tag{34}$$

For simplicity, we remove the bars from Eqs. (33) and (34) and get

$$\frac{d^3 w}{dx^3} + \mu_0 \frac{d^2 w}{dx^2} + \gamma \frac{dw}{dx} + \frac{d\mu_0}{dx} \frac{dw}{dx} = P_2, \tag{35}$$

https://doi.org/10.1016/j.heliyon.2019.e01203

$$\left(1+\frac{4}{3}R\right)\frac{d^2\theta}{dx^2}+\gamma \mathrm{Pr}\frac{d\theta}{dx}+\lambda\mu_0\left(\frac{dw}{dx}\right)^2+\lambda\left(\frac{dw}{dx}\right)\frac{d^2w}{dx^2}=0, \tag{36}$$

Where

$$\lambda=\frac{W_\infty^2\mu_0}{k(\theta_0-\theta_\infty)},\ \gamma=\frac{\rho a_0 W_\infty^2}{\mu_0^2},\ w=\frac{v_0}{W_\infty},$$

$$Pr=\frac{\mu_0^* C_p}{k},\ E=\frac{W_\infty^2}{C_p(\theta_0-\theta_\infty)},\ \gamma Pr=\frac{\rho c a_0 W_\infty^2}{k\mu_0}w^2,\ R=\frac{4\sigma^*\theta_\infty^3}{KK^*}. \tag{37}$$

The suitable non-dimensional boundary conditions are

$$w(0)=0, \tag{38}$$

$$\mathrm{w}\to 1\ as\ x\to\infty, \tag{39}$$

$$\frac{dw}{dx}\to 0\ as\ x\to\infty, \tag{40}$$

and

$$\theta(0)=1, \tag{41}$$

$$\theta\to 1\ \ as\ x\to\infty. \tag{42}$$

Solution for insulated plate

In this case, we have dimensionless parameter of temperature

$$\theta^*=\frac{\theta-\theta_\infty}{\theta_b-\theta_\infty}, \tag{43}$$

where θ_b can be considered the bulk temperature and all other remaining important dimensionless parameters are similar as given above in Eq. (37) The Eckert number is

$$E^*=\frac{W_\infty^2}{c(\theta_b-\theta_\infty)}. \tag{44}$$

The suitable non-dimensional boundary conditions are

$$\left.\frac{d\theta}{dx}\right|_{x\to 0}=0, \tag{45}$$

$$\theta(x)\to\theta_\infty\ \ as\ x\to\infty. \tag{46}$$

We have removed the bars and stars for our simplicity, all quantities are non-dimensional.

https://doi.org/10.1016/j.heliyon.2019.e01203

Skin friction and Nusselt number of fluid flow are expressed as

$$C_f = \frac{\tau_w}{\frac{1}{2}\rho W^2},\ Sh_x \frac{xq_m}{D_B(\varphi_w - \varphi_\infty)}\ \ and\ \ Nu = \frac{xq_w}{k(T_v - T_\infty)}. \tag{47}$$

In above equation skin friction is denoted by C_f and Nusselt number is shown as Nu. Here, τ_w represents wall shear stress and q_w indicates wall heat flux that are explained as

$$\tau_w = \left[\mu_0 \frac{dw}{dx} + a_0 v_0 \frac{d^2w}{dx^2}\right]_{y\to 0},\ \ q_w = -k\left(\frac{\partial \varphi}{\partial x}\right)_{x\to 0},\ \ q_w = -k\left(\frac{\partial \theta}{\partial x}\right)_{x\to 0}, \tag{48}$$

by using dimensionless transformation, we get

$$\frac{1}{2}C_f Re = (1 - M\theta)w'(0) + w''(0),\ Sh_x = -\varphi\prime(0),\ \ Nu = -\theta'(0) \tag{49}$$

Here, Re represents Reynold number.

2.1. Reynolds' model

In this model, the viscosity is expressed in the form

$$\mu_0 = e^{-M\theta} \tag{50}$$

which by Maclaurin's series can be written as

$$\mu_0 = 1 - M\theta \tag{51}$$

Using the value of μ_0 in Eqs. (35) and (36) we obtain

$$\frac{d^3w}{dx^3} + \frac{d^2w}{dx^2} - M\theta\frac{d^2w}{dx^2} + \gamma\frac{dw}{dx} - M\frac{d\theta}{dx}\frac{dw}{dx} = P_2, \tag{52}$$

$$\left(1 + \frac{4}{3}R\right)\frac{d^2\theta}{dx^2} + \gamma \mathrm{Pr}\frac{d\theta}{dx} + \lambda\left(\frac{dw}{dx}\right)^2 - \lambda M\theta\left(\frac{dw}{dx}\right)^2 + \lambda\left(\frac{dw}{dx}\right)\frac{d^2w}{dx^2} = 0. \tag{53}$$

2.2. Vogel's model

In this model,

$$\mu_0 = \mu_0^*\ exp\left(\frac{A}{(B + \theta)} - \theta_v\right) \tag{54}$$

Above equation can be written in the form

https://doi.org/10.1016/j.heliyon.2019.e01203

$$\mu_0 = -\frac{C}{C^*}\left(1 - \frac{A\theta}{B^2}\right), \tag{55}$$

using Eq. (53) in Eqs. (35) and (36) we get

$$\frac{d^3w}{dx^3} + \frac{C}{C^*}\frac{d^2w}{dx^2} - \frac{AC}{C^*B^2}\frac{d^2w}{dx^2} + \gamma\frac{dw}{dx} - \frac{AC}{C^*B^2}\frac{d\theta}{dx}\frac{dw}{dx} = P_2, \tag{56}$$

$$\left(1 + \frac{4}{3}R\right)\frac{d^2\theta}{dx^2} + \gamma \mathrm{Pr}\frac{d\theta}{dx} + \lambda\frac{C}{C^*}\left(\frac{dw}{dx}\right)^2 - \lambda\frac{AC}{C^*B^2}\theta\left(\frac{dw}{dx}\right)^2 + \lambda\left(\frac{dw}{dx}\right)\frac{d^2w}{dx^2} = 0. \tag{57}$$

3. Methodology

The governing partial differential equations which are highly non-linear are transfigured to ordinary differential equations by using suitable transformations with shooting technique is used along with Runge Kutta scheme [32,33,34, 35]. Runge-Kutta method is a technique that solves the initial value problems. First of all we covert momentum and energy equations in first order form.

3.1. Solution for Reynold's model

In this case, Eqs. (50) and (51) for the above mentioned desired form is

$$w''' = -\gamma w' - (1 - M\theta)w\prime\prime + M\theta' w', \tag{58}$$

$$\theta'' = \frac{1}{\left(1 + \frac{4}{3}R\right)}\left(-\gamma Pr\theta' - \lambda(w')^2 - \lambda w\prime w\prime\prime\right). \tag{59}$$

Now, we define new variables to get first order equations from higher order ordinary differential equations.

$$w = l_1,\ w' = l_2,\ \ w'' = l_3,\ \ w''' = l_3',\ \ \theta = l_4,\ \ \theta' = l_5,\ \ \theta'' = l_5'. \tag{60}$$

We get the new system as:

$$l\prime_1 = l_2,\ \ l\prime_2 = l_3,\ \ l\prime_4 = l_5, \tag{61}$$

$$l_3', = -\gamma w' - (1 - M\theta) + M\theta' w', \tag{62}$$

$$l_5' = \frac{1}{\left(1 + \frac{4}{3}R\right)}\left(-\gamma Pr\theta' - \lambda(w')^2 - \lambda w\prime w\prime\prime\right). \tag{63}$$

Along with boundary conditions

https://doi.org/10.1016/j.heliyon.2019.e01203

$$l_1(0)=0,\ l_1(\infty)=1,\ l_2(0)=1,\ l_2(\infty)=0,\ l_4(0)=1,\ l_4(\infty)=0. \tag{64}$$

3.2. Solution for Vogel's model

In this procedure, Eqs. (54) and (55) gets the form

$$w'''=-\gamma w'-\left(1-\frac{A}{B^2}\right)\frac{C}{C^*}w''+\frac{AC}{C^*B^2}\theta' w', \tag{65}$$

$$\theta''=\frac{1}{\left(1+\frac{4}{3}R\right)}\left(-\gamma Pr\theta'-\left(1+\frac{A\theta}{B^2}\right)\frac{C}{C^*}\lambda(w')^2-\lambda w'w''\right). \tag{66}$$

As in above case, we have

$$l_3'=-\gamma w'-\left(1-\frac{A}{B^2}\right)\frac{C}{C^*}w''+\frac{AC}{C^*B^2}\theta' w', \tag{67}$$

$$l_5'=\frac{1}{\left(1+\frac{4}{3}R\right)}\left(-\gamma Pr\theta'-\left(1+\frac{A\theta}{B^2}\right)\frac{C}{C^*}\lambda(w')^2-\lambda w'w''\right), \tag{68}$$

along with boundary conditions of the problem as described in Eq. (64).

4. Results & discussion

In the realm of graphical portray, impact of physical parameters on temperature and velocity profiles are canvassed briefly. Fig. 2 renders the effect of λ on temperature for Reynolds' model. Fig. 3 depicts the behavior of temperature against γ for Reynold's model. Temperature profile is going down by rising γ. Fig. 4 delineates the outcome on velocity field for Reynolds' model on M. The velocity field decreases with the increment of M. Fig. 5 describes the Pr on temperature distribution for Reynolds' model. Fig. 6 shows the effect of γ on velocity for Reynolds' model. Fig. 7 draws the consequences of C for velocity distribution of Vogel's model. The profile enhances by escalating C. Fig. 8 gives the temperature profile on A for Vogel's model. Fig. 9 shows the impact on velocity for A on Vogel's model. Fig. 10 delineates the behavior on M for temperature field of Reynolds' model. Fig. 11 describes effects of B on velocity profile of Vogel's model. Figs. 12 and 13 indicates effects of B and C^* for temperature of Vogel's model. Fig. 14 draws the consequences of C on velocity distribution for Vogel's model. Fig. 15 describes the influence of Pr on temperature of Vogel's model. Fig. 16 describes the effects on velocity field of Vogel's model. Fig. 17 depicts the effects of γ for velocity of Vogel's model. Fig. 18 shows that temperature of γ gives lower behavior for Vogel's model. Fig. 19 depicts that A and γ decreases skin friction for Vogel's model. Fig. 20 displays that consequences of γ and A on Nusselt number goes down due to accretion in λ. Fig. 21 explicates the effects of γ and M on Nusselt number grows for Reynolds' model. Figs. 22, 23, and

https://doi.org/10.1016/j.heliyon.2019.e01203

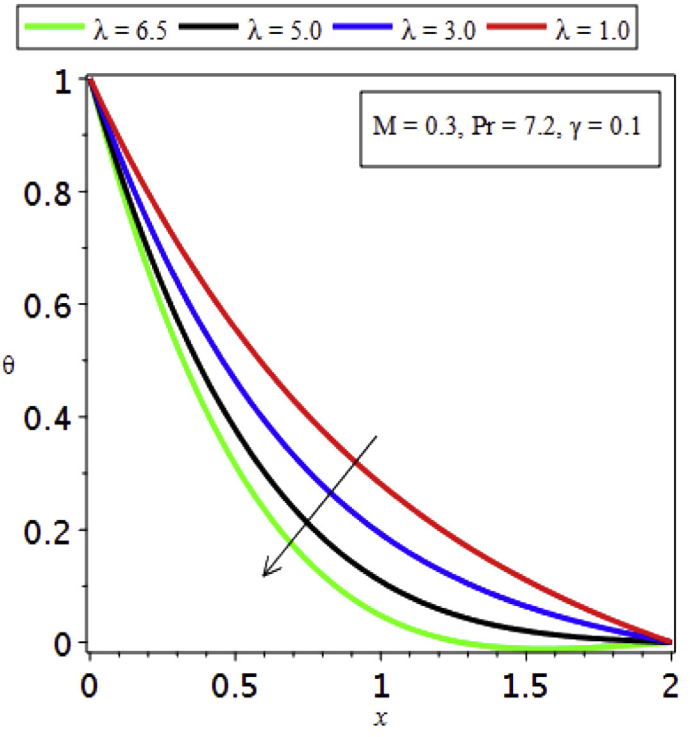

Fig. 2. Influence of λ on Temperature profile for Reynolds' model.

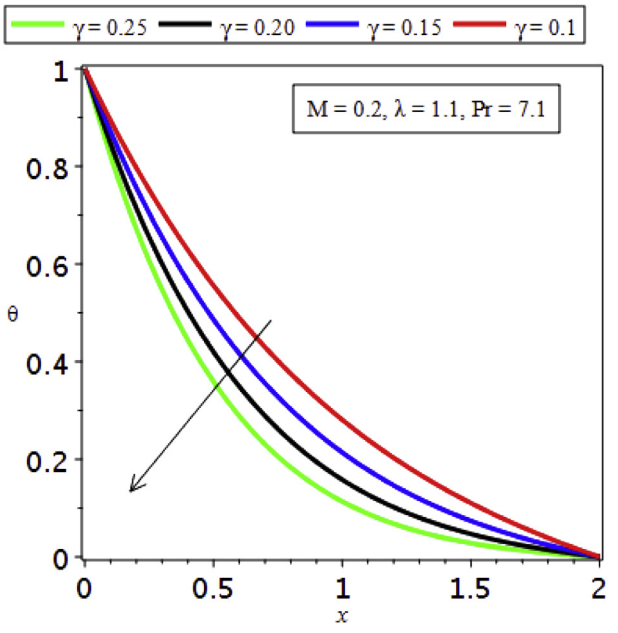

Fig. 3. Effects of γ on Temperature field for Reynolds' model.

https://doi.org/10.1016/j.heliyon.2019.e01203

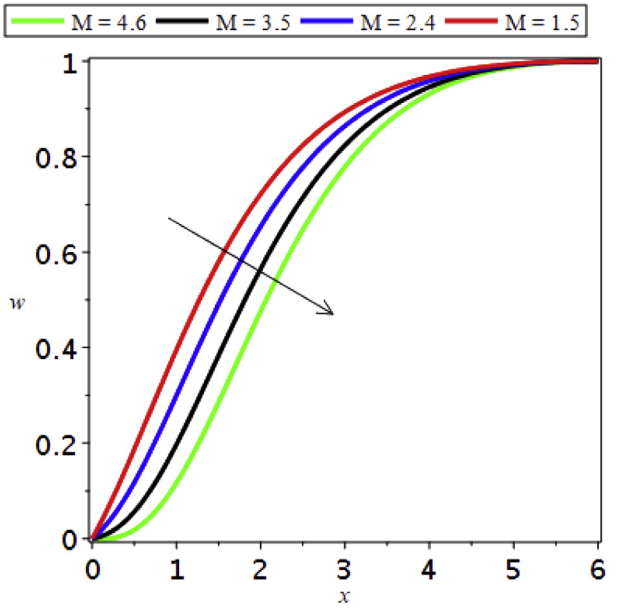

Fig. 4. Impress of M for Velocity profile of Reynolds' model.

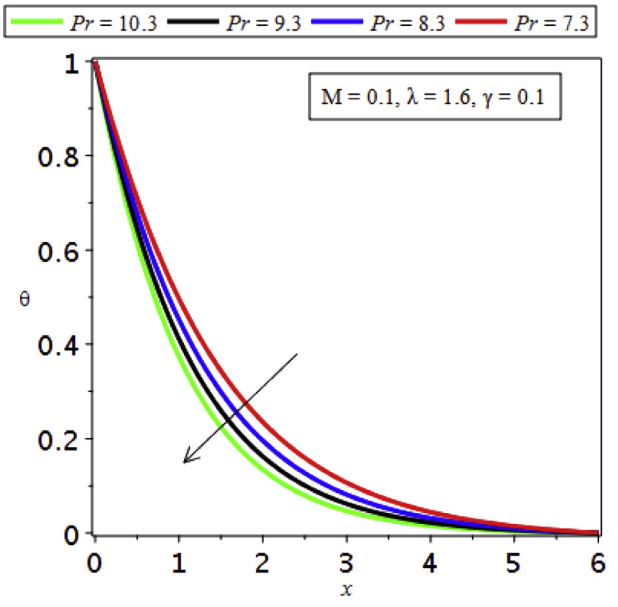

Fig. 5. Impact of Pr for Temperature outline of Reynolds' model.

https://doi.org/10.1016/j.heliyon.2019.e01203

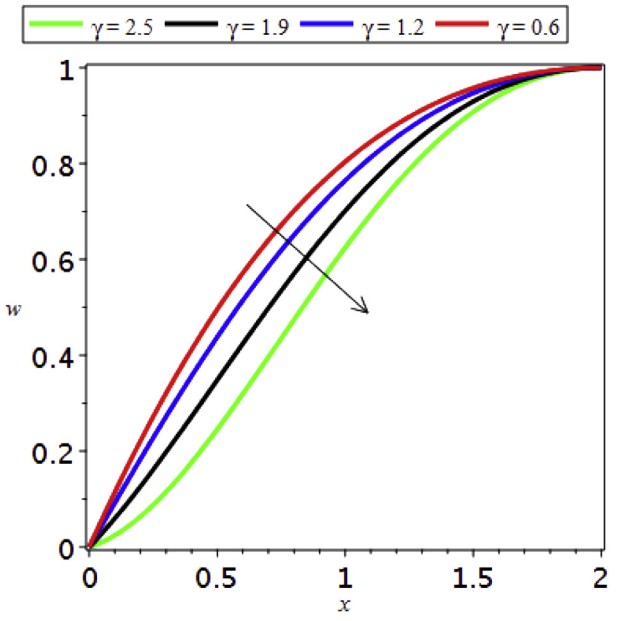

Fig. 6. Affect of γ for Velocity silhouette of Reynolds' model.

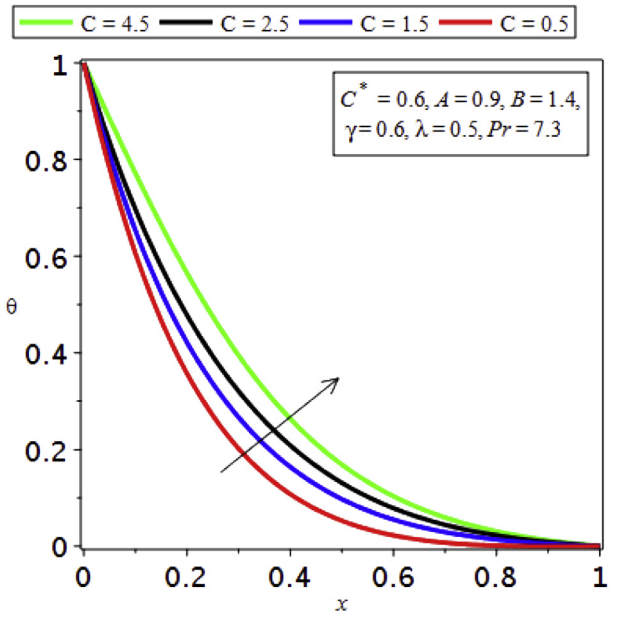

Fig. 7. Sway of C on Temperature contour for Vogel's model.

https://doi.org/10.1016/j.heliyon.2019.e01203

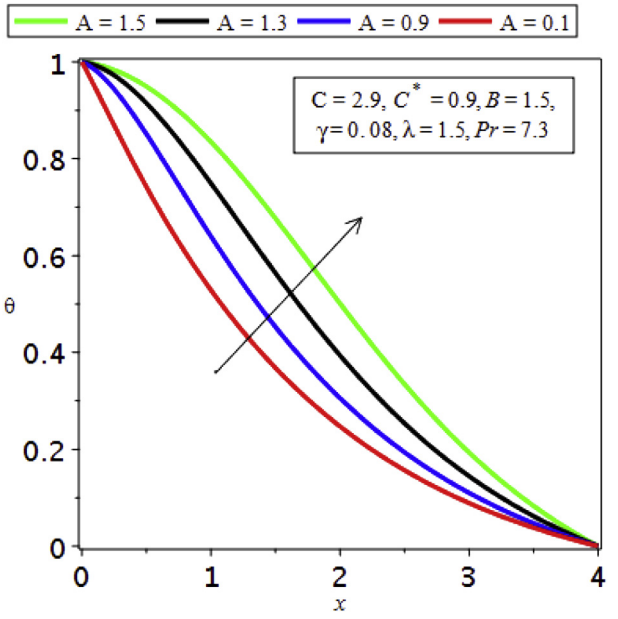

Fig. 8. Movement of A on Temperature profile for Vogel's model.

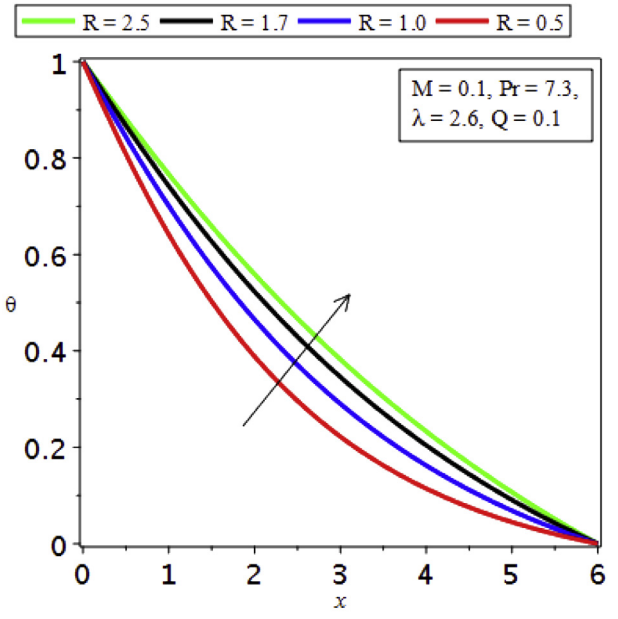

Fig. 9. Influence of R on Temperature field for Vogel's model.

https://doi.org/10.1016/j.heliyon.2019.e01203

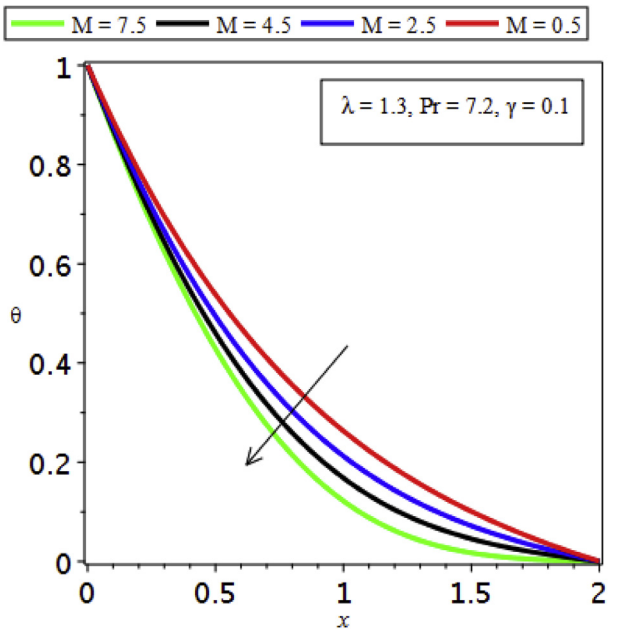

Fig. 10. Effect of M onTemperature outline for Reynolds' model.

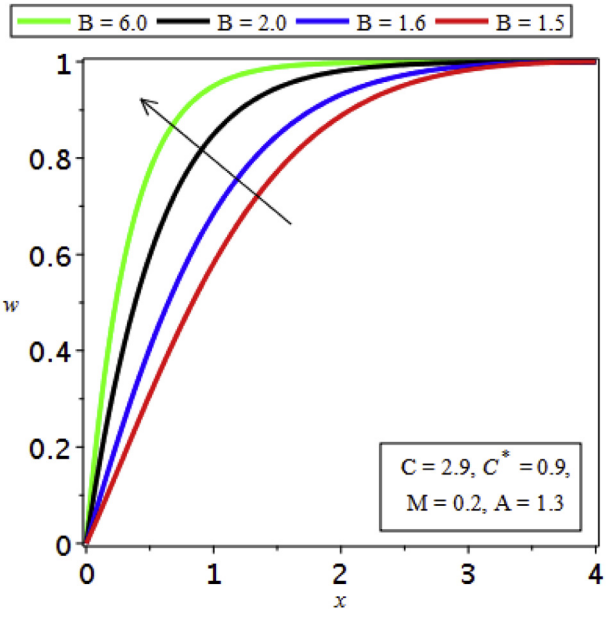

Fig. 11. Impact of B on Velocity field for Vegol's model.

https://doi.org/10.1016/j.heliyon.2019.e01203

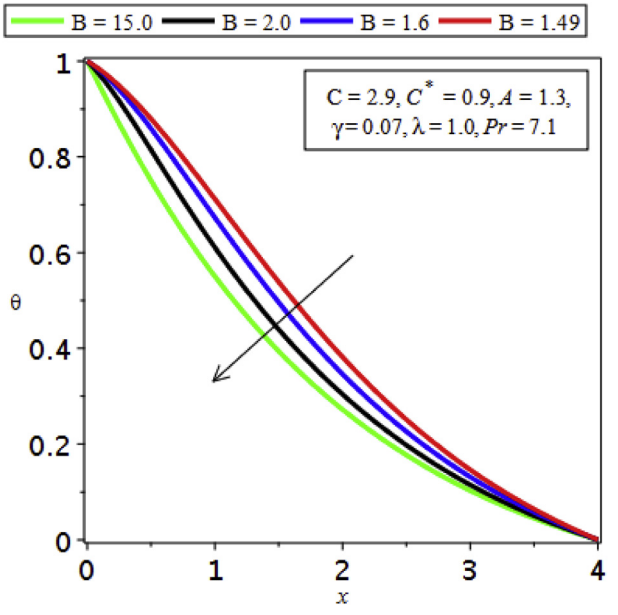

Fig. 12. Affect of B on Temperature profile for Vogel's model.

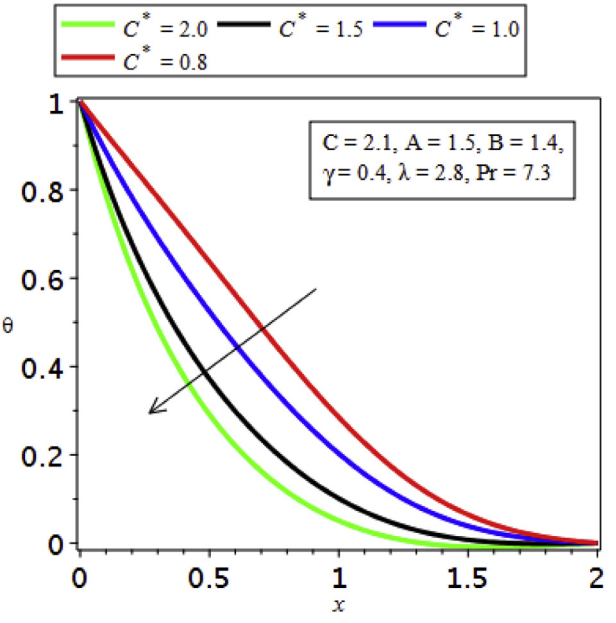

Fig. 13. Influence of C^* on Temperature field for Vogel's model.

https://doi.org/10.1016/j.heliyon.2019.e01203

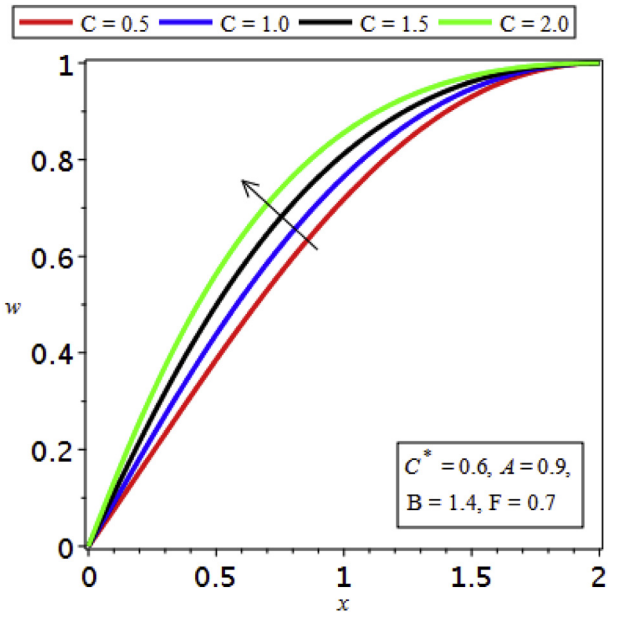

Fig. 14. Influence of C on Velocity profile for Vogel's model.

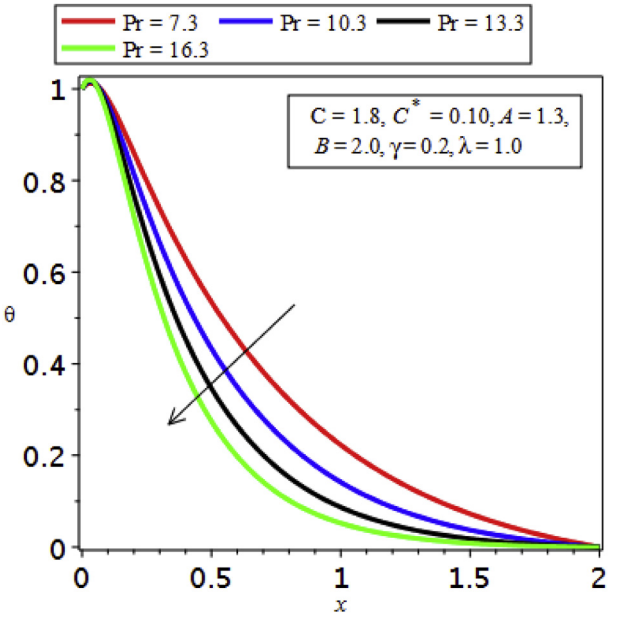

Fig. 15. Impact of Pr for Temperature outline for Vogel's model.

https://doi.org/10.1016/j.heliyon.2019.e01203

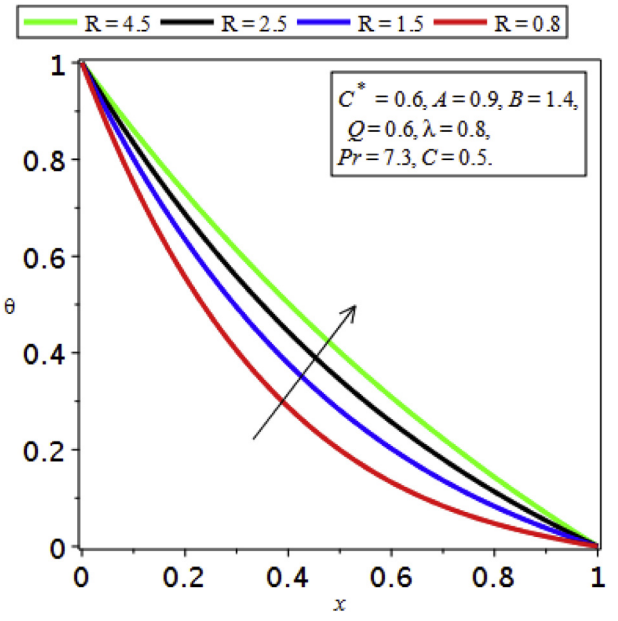

Fig. 16. Effect of R for Temperature field for Vogel's model.

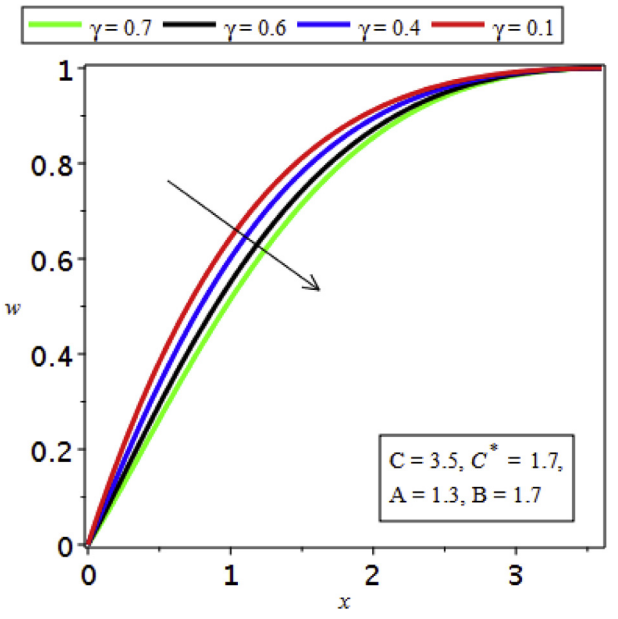

Fig. 17. Impact of γ on Velocity field for Vogel's model.

https://doi.org/10.1016/j.heliyon.2019.e01203

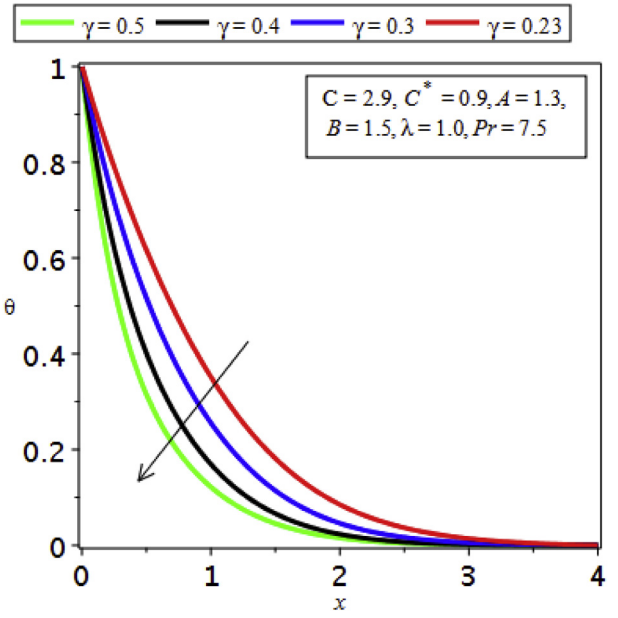

Fig. 18. Effect of γ on Temperature outline for Vogel's model.

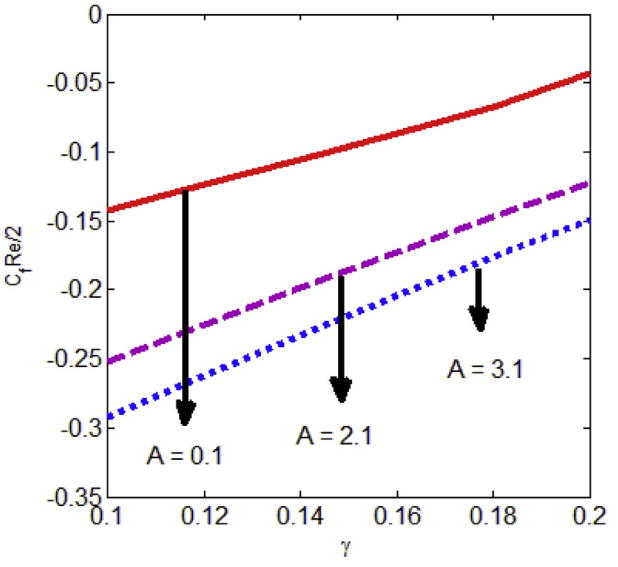

Fig. 19. Effect of γ and A on skin friction for Vogel's model.

https://doi.org/10.1016/j.heliyon.2019.e01203

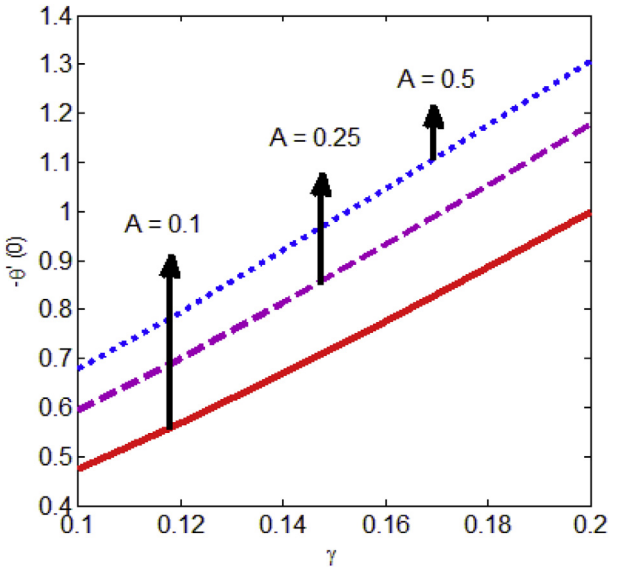

Fig. 20. Influence of γ and A on Nusselt number for Vogel's model.

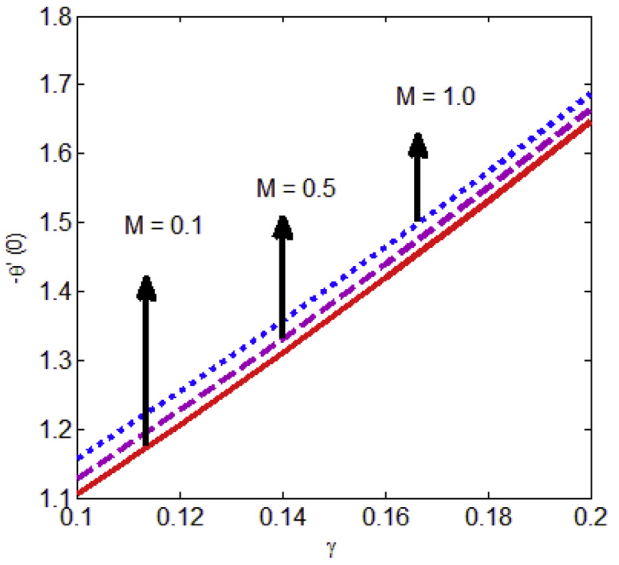

Fig. 21. Impact of γ and M on Nusselt number for Reynolds' model.

https://doi.org/10.1016/j.heliyon.2019.e01203

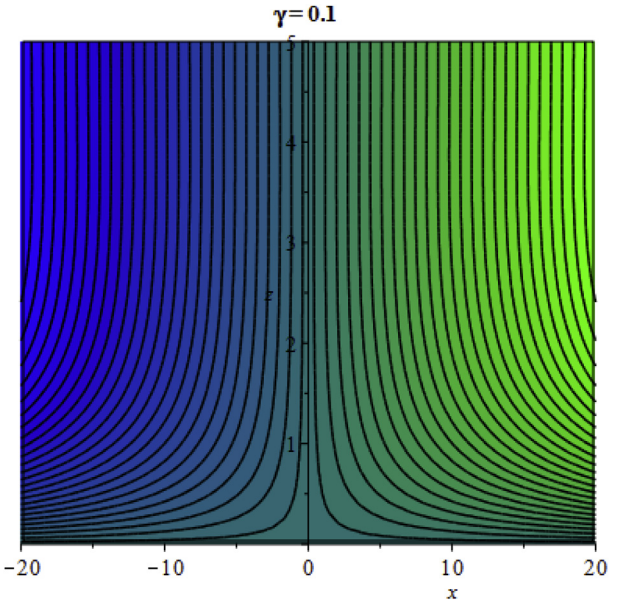

Fig. 22. Stream lines for $\gamma = 0.1$ for Reynolds' model.

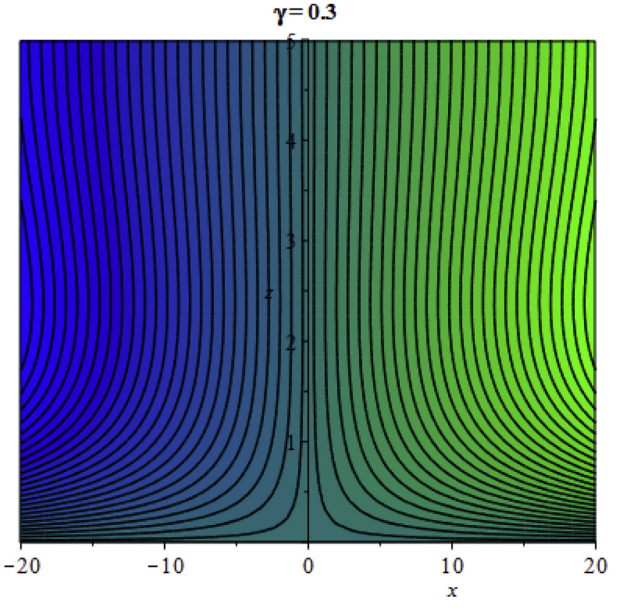

Fig. 23. Stream lines for $\gamma = 0.3$ for Reynolds' model.

https://doi.org/10.1016/j.heliyon.2019.e01203

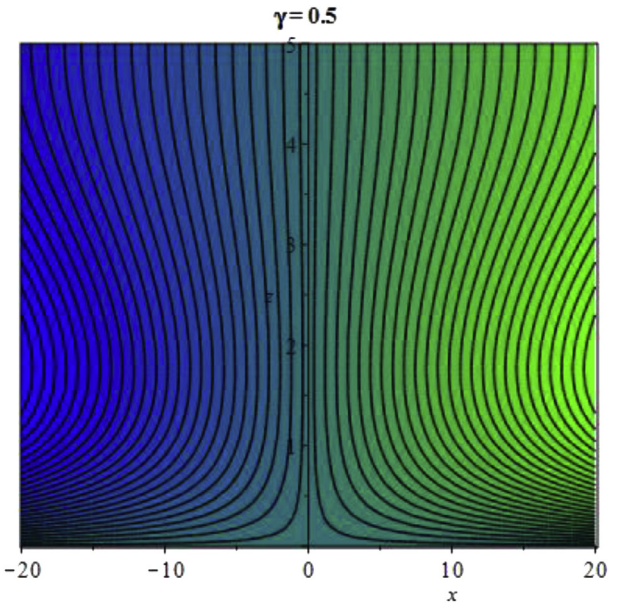

Fig. 24. Stream lines for $\gamma = 0.5$ for Reynolds' model.

24 clarify stream lines graphs for different values of γ for Reynolds' model. Figs. 25, 26, and 27 clarify the three dimensional graphs for different values of γ for Reynolds' model. Table 1 represents behavior of $A,\ B,\ C,\ R\ F\ \gamma\ \lambda$ and Pr on Nusselt number. Tables 2, 3, 4, 5, 6, 7, 8, 9, 10, 11, 12, 13, and 14 shows values of $\frac{d\theta}{dx}$ for M,

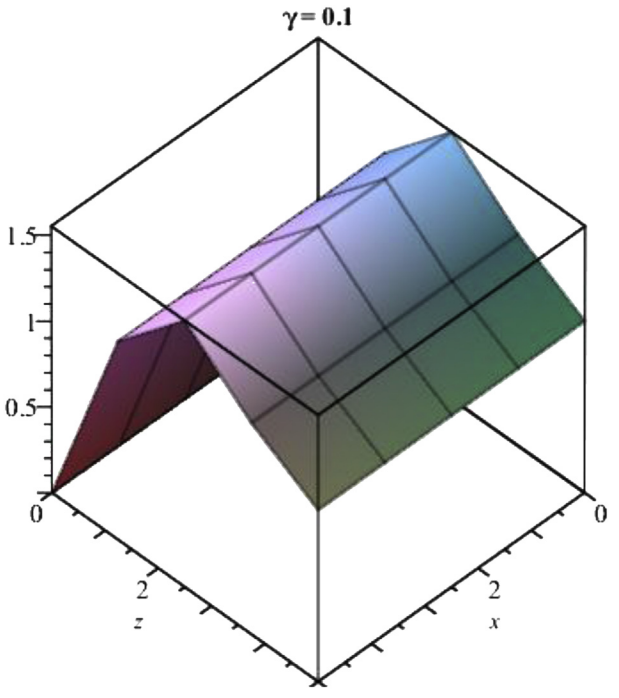

Fig. 25. Three dimensional graph of $w(x)$ for $\gamma = 0.1$.

https://doi.org/10.1016/j.heliyon.2019.e01203

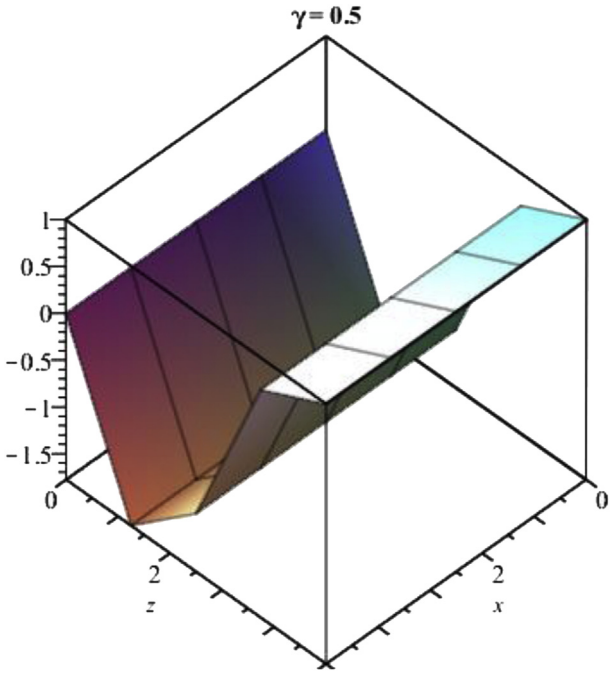

Fig. 26. Three dimensional graph of $w(x)$ for $\gamma = 0.5$.

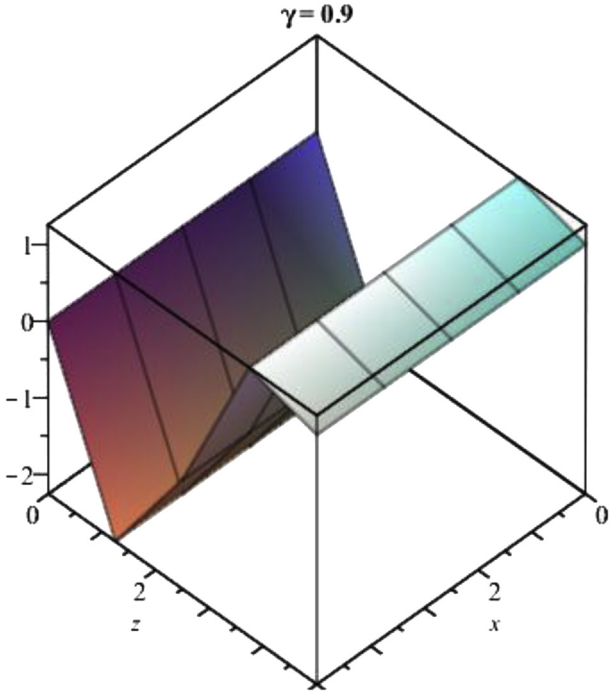

Fig. 27. Three dimensional graph of $w(x)$ for $\gamma = 0.9$.

https://doi.org/10.1016/j.heliyon.2019.e01203

Table 1. Values for Nusselt number of distinct parameters for Vogels' model.

γ	Pr	λ	*C*	*B*	C^*	*A*	*R*	− θ'(0)
0.1	7.2	1.5	2.9	1.5	0.9	0.08	0.8	0.61675
0.2	7.2	1.5	2.9	1.5	0.9	0.08	0.8	0.72213
0.3	7.2	1.5	2.9	1.5	0.9	0.08	0.8	0.77681
0.1	7.2	1.5	2.9	1.5	0.9	0.08	0.8	0.61675
0.1	7.3	1.5	2.9	1.5	0.9	0.08	0.8	0.62488
0.1	7.4	1.5	2.9	1.5	0.9	0.08	0.8	0.63304
0.1	7.2	1.5	2.9	1.5	0.9	0.08	0.8	0.61675
0.1	7.2	1.6	2.9	1.5	0.9	0.08	0.8	0.60731
0.1	7.2	1.7	2.9	1.5	0.9	0.08	0.8	0.59791
0.1	7.2	1.5	2.9	1.5	0.9	0.08	0.8	0.61675
0.1	7.2	1.5	3.0	1.5	0.9	0.08	0.8	0.61376
0.1	7.2	1.5	3.1	1.5	0.9	0.08	0.8	0.61077
0.1	7.2	1.5	2.9	1.5	0.9	0.08	0.8	0.61675
0.1	7.2	1.5	2.9	1.6	0.9	0.08	0.8	0.62246
0.1	7.2	1.5	2.9	1.7	0.9	0.08	0.8	0.62974
0.1	7.2	1.5	2.9	1.5	0.9	0.08	0.8	0.61675
0.1	7.2	1.5	2.9	1.5	0.1	0.08	0.8	0.62974
0.1	7.2	1.5	2.9	1.5	0.2	0.08	0.8	0.59990
0.1	7.2	1.5	2.9	1.5	0.9	0.08	0.8	0.61675
0.1	7.2	1.5	2.9	1.5	0.9	0.09	0.8	0.60350
0.1	7.2	1.5	2.9	1.5	0.9	0.10	0.8	0.59456
0.1	7.2	1.5	2.9	1.5	0.9	0.08	0.8	0.61675
0.1	7.2	1.5	2.9	1.5	0.9	0.08	0.9	0.78562
0.1	7.2	1.5	2.9	1.5	0.9	0.08	1.0	0.85214
0.1	7.2	1.5	2.9	1.5	0.9	0.08	0.8	0.61675

Table 2. Values of $\frac{d\theta}{dx}$ at the wall for λ for Reynolds' model.

λ	R	M	Pr	γ	*Results*
1.0	0.5	0.3	7.2	0.1	−.1108
3.0	0.5	0.3	7.2	0.1	−1.427
5.0	0.5	0.3	7.2	0.1	−1.732
6.5	0.5	0.3	7.2	0.1	−1.952

https://doi.org/10.1016/j.heliyon.2019.e01203

Table 3. Values of $\frac{d\theta}{dx}$ at the wall for M for Reynolds' model.

M	**R**	λ	Pr	γ	***Results***
0.5	0.5	1.0	7.2	0.1	−.701
2.5	0.5	1.0	7.2	0.1	−1.284
4.5	0.5	1.0	7.2	0.1	−1.359
7.5	0.5	1.0	7.2	0.1	−1.416

Table 4. Values of $\frac{d\theta}{dx}$ at the wall for Pr for Reynolds' model.

Pr	**R**	λ	**M**	γ	***Results***
7.3	0.5	1.0	0.3	0.1	−0.666
8.3	0.5	1.0	0.3	0.1	−0.762
9.3	0.5	1.0	0.3	0.1	−0.860
10.3	0.5	1.0	0.3	0.1	−0.958

Table 5. Values of $\frac{d\theta}{dx}$ at the wall for γ for Reynolds' model.

γ	**R**	λ	**M**	Pr	***Results***
0.1	0.5	1.0	0.3	7.2	−1.111
0.15	0.5	1.0	0.3	7.2	−1.370
0.2	0.5	1.0	0.3	7.2	−1.653
0.25	0.5	1.0	0.3	7.2	−1.954

Table 6. Values of $\frac{d\theta}{dx}$ at the wall for **R** for Reynolds' model.

R	γ	λ	**M**	Pr	***Results***
0.5	0.1	1.0	0.3	7.2	−1.111
0.6	0.1	1.0	0.3	7.2	−1.126
0.7	0.1	1.0	0.3	7.2	−1.135
0.8	0.1	1.0	0.3	7.2	−1.147

Table 7. Values of $\frac{d\theta}{dx}$ at the wall for γ for Vogels' model.

γ	***C***	C^*	***A***	***B***	***R***	λ	Pr	***Results***
0.23	2.9	0.9	1.3	1.5	0.8	1.0	7.5	−0.932
0.3	2.9	0.9	1.3	1.5	0.8	1.0	7.5	−1.363
0.4	2.9	0.9	1.3	1.5	0.8	1.0	7.5	−2.026
0.5	2.9	0.9	1.3	1.5	0.8	1.0	7.5	−2.724

https://doi.org/10.1016/j.heliyon.2019.e01203

Table 8. Values of $\frac{d\theta}{dx}$ at the wall for ***Pr*** for Vogels' model.

Pr	*C*	C^*	*A*	*B*	*R*	Λ	γ	*Results*
7.3	2.9	0.9	1.3	1.5	0.8	1.0	0.23	0.846
10.3	2.9	0.9	1.3	1.5	0.8	1.0	0.23	1.084
13.3	2.9	0.9	1.3	1.5	0.8	1.0	0.23	1.314
16.3	2.9	0.9	1.3	1.5	0.8	1.0	0.23	1.526

Table 9. Values of $\frac{d\theta}{dx}$ at the wall for γ for Vogels' model.

λ	*C*	C^*	*A*	*B*	*R*	γ	Pr	*Results*
1.0	2.9	0.9	1.3	1.5	0.8	0.23	7.5	−0.502
2.0	2.9	0.9	1.3	1.5	0.8	0.23	7.5	−0.281
3.4	2.9	0.9	1.3	1.5	0.8	0.23	7.5	−0.166
4.5	2.9	0.9	1.3	1.5	0.8	0.23	7.5	−0.053

Table 10. Values of $\frac{d\theta}{dx}$ at the wall for $\boldsymbol{C^*}$ for Vogels' model.

C^*	*C*	λ	*A*	*B*	*R*	γ	Pr	*Results*
0.8	2.9	1.0	1.3	1.5	0.8	0.23	7.5	−0.146
1.0	2.9	1.0	1.3	1.5	0.8	0.23	7.5	−0.223
1.5	2.9	1.0	1.3	1.5	0.8	0.23	7.5	−1.974
2.0	2.9	1.0	1.3	1.5	0.8	0.23	7.5	−2.394

Table 11. Values of $\frac{d\theta}{dx}$ at the wall for ***C*** for Vogels' model.

C	C^*	λ	*A*	*B*	*R*	γ	Pr	*Results*
0.5	0.9	1.0	1.3	1.5	0.8	0.23	7.5	−5.044
1.0	0.9	1.0	1.3	1.5	0.8	0.23	7.5	−4.622
1.5	0.9	1.0	1.3	1.5	0.8	0.23	7.5	−3.566
2.0	0.9	1.0	1.3	1.5	0.8	0.23	7.5	−0.535

Table 12. Values of $\frac{d\theta}{dx}$ at the wall for ***B*** for Vogels' model.

B	C^*	λ	*A*	*C*	*R*	γ	Pr	*Results*
1.49	0.9	1.0	1.3	2.9	0.8	0.23	7.5	−0.160
1.6	0.9	1.0	1.3	2.9	0.8	0.23	7.5	−0.206
2.0	0.9	1.0	1.3	2.9	0.8	0.23	7.5	−0.262
15.0	0.9	1.0	1.3	2.9	0.8	0.23	7.5	−0.535

https://doi.org/10.1016/j.heliyon.2019.e01203

Table 13. Values of $\frac{d\theta}{dx}$ at the wall for **A** for Vogels' model.

A	C^*	λ	*B*	*C*	*R*	γ	Pr	*Results*
0.8	0.9	1.0	1.5	2.9	0.1	0.23	7.5	−0.160
0.9	0.9	1.0	1.5	2.9	0.1	0.23	7.5	−0.206
1.3	0.9	1.0	1.5	2.9	0.1	0.23	7.5	−0.262
1.5	0.9	1.0	1.5	2.9	0.1	0.23	7.5	−0.535

Table 14. Values of $\frac{d\theta}{dx}$ at the wall for **R** for Vogels' model.

R	C^*	λ	*B*	*C*	*A*	γ	Pr	*Results*
0.8	0.9	1.0	1.5	2.9	0.1	0.23	7.5	−0.160
0.9	0.9	1.0	1.5	2.9	0.1	0.23	7.5	−0.267
1.0	0.9	1.0	1.5	2.9	0.1	0.23	7.5	−0.374
1.1	0.9	1.0	1.5	2.9	0.1	0.23	7.5	−0.481

Table 15. Values of skin friction coefficient for A and γ for Vogels' model.

γ	A	λ	*C*	*B*	C^*	*Pr*	$\frac{1}{2}C_f Re$
0.1	1.3	1.5	3.5	1.7	1.7	7.3	0.42382
0.2	1.3	1.5	3.5	1.7	1.7	7.3	0.63031
0.3	1.3	1.5	3.5	1.7	1.7	7.3	0.78747
0.1	1.3	1.5	3.5	1.7	1.7	7.3	0.42382
0.1	1.4	1.5	3.5	1.7	1.7	7.3	0.48943
0.1	1.5	1.5	3.5	1.7	1.7	7.3	0.54517
0.1	1.3	1.5	3.5	1.7	1.7	7.3	0.42382
0.1	1.3	1.6	3.5	1.7	1.7	7.3	0.43324
0.1	1.3	1.7	3.5	1.7	1.7	7.3	0.42907
0.1	1.3	1.5	3.5	1.7	1.7	7.3	0.42382
0.1	1.3	1.5	3.6	1.7	1.7	7.3	0.40182
0.1	1.3	1.5	3.7	1.7	1.7	7.3	0.38175
0.1	1.3	1.5	3.5	1.7	1.7	7.3	0.42382
0.1	1.3	1.5	3.5	1.8	1.7	7.3	0.30023
0.1	1.3	1.5	3.5	1.9	1.7	7.3	0.17688
0.1	1.3	1.5	3.5	1.6	1.7	7.3	0.42382
0.1	1.3	1.5	3.5	1.7	1.8	7.3	0.43749
0.1	1.3	1.5	3.5	1.7	1.9	7.3	0.46459
0.1	1.3	1.5	3.5	1.7	1.7	7.3	0.42382
0.1	1.3	1.5	3.5	1.7	1.7	7.3	0.43532
0.1	1.3	1.5	3.5	1.7	1.7	7.4	0.543727
0.1	1.3	1.5	3.5	1.7	1.7	7.5	0.42382

https://doi.org/10.1016/j.heliyon.2019.e01203

B, C, R, γ, λ C^*, A, λ and Pr for both models. Table 15 explicates the consequences on skin friction coefficient for M and γ which is escalating with the accretion in the values of γ.

5. Conclusions

An exploration has been implemented to interrogate the study of Reynolds' and Vogel's viscosity models for the flow of a viscoelastic fluid. Using the similarity transformation governing equations are transmuted into ordinary differential equations. The numerical solution is obtained. Consequences of all different parameters on temperature and velocity fields are interrogated to probe the comportment of fluid's flow. Parameter's sway on temperature and velocity are explored with tables and graphs. The significant points of the findings of the present study are as follows:

1) An apprehensible excrescency is sighted in velocity portray with increasing C and reduction occurs in velocity curve due to increment in curvature parameter γ , A and M on Vogel's and Reynolds' models.
2) The temperature of both models decreases due to escalation of γ and Pr.
3) Stream lines compresses and 3D graphs crooked due to increase in γ of Reynold's model.
4) Skin friction graph is explicating the lower behavior because of increasing A and Nusselt number graph increases by change in A.

Declarations

Author contribution statement

Azad Hussain: Analyzed and interpreted the data; Contributed analysis tools or data.

Sobia Akbar, Lubna Sarwar: Conceived and designed the analysis; Contributed analysis tools or data; Wrote the paper.

Sohail Nadeem, Zaffar Iqbal: Contributed analysis tools or data; Wrote the paper.

Funding statement

This research did not receive any specific grant from funding agencies in the public, commercial, or not-for-profit sectors.

Competing interest statement

The authors declare no conflict of interest.

https://doi.org/10.1016/j.heliyon.2019.e01203

Additional information

No additional information is available for this paper.

References

[1] Rehmat Ellahi, Arshad Riaz, Analytical solutions for MHD flow in a third-grade fluid with variable viscosity, Math. Comput. Model. 52 (2010) 1783−1793.

[2] Sohail Nadeem, Changhoon Lee, Boundary layer flow of nanofluid over an exponentially stretching surface, Nanoscale Res. Lett. 7 (2012) 94.

[3] Khalil Ur Rehman, Aneeqa Ashfaq Malik, M.Y. Malik, Noor Ul Saba, Mutual effects of thermal radiations and thermal stratification on tangent hyperbolic fluid flow yields by both cylindrical and flat surfaces, Case Stud. Thermal Eng. 7 (2017) 244−254.

[4] N.S. Akbar, S. Nadeem, R.U. Haq, Z.H. Khan, Radiation effects on MHD stagnation point flow of nano fluid towards a stretching surface with convective boundary condition, Chin. J. Aeronaut. 26 (6) (2013) 1389−1397.

[5] T. Salahuddin, M.Y. Malik, Arif Hussain, Muhammad Awais, Imad Khan, Mair Khan, Analysis of tangent hyperbolic nanofluid impinging on a stretching cylinder near the stagnation point, Results in Physics (2017) 426−434.

[6] S. Bilal, M.Y. Malik, M. Awais, Khalil Ur Rehman, Arif Hussain, I. Khan, Numerical investigation on 2D viscoelastic fluid due to exponentially stretching surface with magnetic effects: an application of non-Fourier flux theory, Neural Comput. Appl. (2016).

[7] Sohail Nadeem, Shehla Zaheer, Tiegang Fang, Effects of thermal radiation on the boundary layer flow of a Jeffrey fluid over an exponentially stretching surface, Numer. Algorithm. 57 (2011) 187−205.

[8] M.M. Bhatti, A. Zeeshan, N. Ijaz, O. Anwar Bég, A. Kadir, Mathematical modelling of nonlinear thermal radiation effects on EMHD peristaltic pumping of viscoelastic dusty fluid through a porous medium duct, Eng. Sci. Technol. Int. J. (2016).

[9] Mair Khan, M.Y. Malik, T. Salahuddin, Heat generation and solar radiation effects on Carreau nanofluid over a stretching sheet with variable thickness: using coefficients improved by Cash and Carp, Res. Phys. 7 (2017) 2512−2519.

https://doi.org/10.1016/j.heliyon.2019.e01203

[10] R. Ellahi, M. Razab, K. Vafaia, Series solutions of non-Newtonian nanofluids with Reynolds' model and Vogel's model by means of the homotopy analysis method, Math. Comput. Model. 55 (2012) 1876–1891.

[11] S. Nadeem, S. Saleem, Mixed convection flow of Eyring–Powell fluid along a rotating cone, Res. Phys. 4 (2014) 54–62.

[12] Kai-Long Hsiao, To promote radiation electrical MHD activation energy thermal extrusion manufacturing system efficiency by using Carreau-nanofluid with parameters control method, Energy 130 (2017) 486–499.

[13] Kai-Long Hsiao, Combined electrical MHD heat transfer thermal extrusion system using Maxwell fluid with radiative and viscous dissipation effects, Appl. Therm. Eng. (2016).

[14] Kai-Long Hsiao, Micropolar nanofluid flow with MHD and viscous dissipation effects towards a stretching sheet with multimedia feature, Int. J. Heat Mass Tran. 112 (2017) 983–990.

[15] Kai-Long Hsiao, Stagnation electrical MHD nanofluid mixed convection with slip boundary on a stretching sheet, Appl. Therm. Eng. 98 (2016) 850–861.

[16] G. Makanda, O.D. Makinde, P. Sibanda, Natural convection of viscoelastic fluid from a cone embedded in a porous medium with viscous dissipation, Math. Probl Eng. (2013), 934712 (11 pages).

[17] W.A. Khan, J.R. Culham, O.D. Makinde, Combined heat and mass transfer of third-grade nanofluids over a convectively-heated stretching permeable surface, Can. J. Chem. Eng. 93 (10) (2015) 1880–1888.

[18] W.A. Khan, R. Culham, O.D. Makinde, Hydromagnetic Blasius flow of power-law nanofluids over a convectively heated vertical plate, Can. J. Chem. Eng. 93 (10) (2015) 1830–1837.

[19] O.D. Makinde, A. Ogulu, The effect of thermal radiation on the heat and mass transfer flow of a variable viscosity fluid past a vertical porous plate permeated by a transverse magnetic field, Chem. Eng. Commun. 195 (12) (2008) 1575–1584.

[20] O.D. Makinde, Effect of variable viscosity on thermal boundary layer over a permeable flat plate with radiation and a convective surface boundary condition, J. Mech. Sci. Technol. 26 (5) (2012) 1615–1622.

https://doi.org/10.1016/j.heliyon.2019.e01203

[21] M. Yurusoy, M. Pakdemirili, Approximte anlytical solutions for flow of a third grade in a pipe, Int. J. Non Lin. Mech. 37 (2002) 187−195.

[22] M. Pakdemirili, B.S. Yilbas, Entropy generation for pipe flow of a third grade fluid with vogel model of viscosity, Int. J. Non Lin. Mech. 41 (2006) 432−437.

[23] W.D. Beard, K. Walters, Elastico-viscous boundary layer flows, Proc. Camb. Philos. Soc. (1964), 60667.

[24] T.B. Chang, A. Mehmood, O.A. Beg, M. Narahari, M.N. Islam, F. Ameen, Numerical study of transient free convective mass transfer in a Walters-B viscoelastic flow with wall suction, Commun. Nonlinear Sci. Numer. Simulat. 16 (2011) 216−225.

[25] M.M. Nandepanavar, M.S. Abel, J.V. Tawade, Heat transfer in a Walter's liquid B fluid over an impermeable stretching sheet with non-uniform heat source/sink and elastic deformation, Commun. Nonlinear Sci. Numer. Simulat. 15 (2010) 1791−1802.

[26] A.K.A. Hakeem, N.V. Ganesh, B. Ganga, Effect of heat radiation in a Walter's liquid B fluid over a stretching sheet with non-uniform heat source/sink and elastic deformation, J. King Saud Univ. Eng. Sci. 26 (2014) 168−175.

[27] S. Nadeem, R. Mehmood, S.S. Motsa, Numerical investigation on MHD oblique flow of Walter's B type nanofluid over a convective surface, Int. J. Therm. Sci. 92 (2015) 162−172.

[28] H. Talla, Numerical study of flow of Walter's liquid B over an exponentially stretching sheet, Int. J. Sci. Res. Publ. 3 (2015) 2250−3153.

[29] K. Ramesh, M. Devakar, Effect of heat transfer on the peristaltic flow of Walter-B fluid in a vertical channel with external magnetic field, J. Aero. Eng. 10 (2015), 04015050.

[30] R. Cortell, Fluid flow and radiative nonlinear heat transfer over a stretching sheet, J. King Saud Univ. Sci. 26 (2) (2014) 161−167.

[31] Mair Khan, M.Y. Malik, T. Salahuddin, Imad Khan, Heat transfer squeezed flow of Carreau fluid over a sensor surface with variable thermal conductivity: a numerical study, Res. Phys. 6 (2016) 940−945.

[32] Arif Hussain, M.Y. Malik, S. Bilal, M. Awais, T. Salahuddin, Computational analysis of magnetohydrodynamic Sisko fluid flow over a stretching cylinder in the presence of viscous dissipation and temperature dependent thermal conductivity, Res. Phys. 7 (2017) 139−146.

https://doi.org/10.1016/j.heliyon.2019.e01203

[33] Arif Hussain, M.Y. Malika, T. Salahuddin, S. Bilal, M. Awais, Combined effects of viscous dissipation and Joule heating on MHD Sisko nanofluid over a stretching cylinder, J. Mol. Liq. 231 (2017) 341−352.

[34] T. Salahuddin, M.Y. Malik, Arif Hussain, Muhammad Awais, Imad Khan, Mair Khan, Analysis of tangent hyperbolic nanofluid impinging on a stretching cylinder near the stagnation point, Res. Phys. 7 (2017) 426−434.

https://doi.org/10.1016/j.heliyon.2019.e01203